Contents lists available at ScienceDirect

Surface Science

Energy-level alignment in the adsorption of phosphonyl reagents on γ-Al₂O₃

V.M. Bermudez *

Electronics Science and Technology Division, Naval Research Laboratory, Washington, DC 20375-5347, USA

ARTICLE INFO

ABSTRACT

Density functional theory is applied to the computation of the adsorption energy (ΔE_{ads}) for a series of molecules on γ-Al₂O₃. Three different cluster models are used to represent the γ-Al₂O₃ surface. The molecules of interest all contain a phosphonyl (P=O) functional group and adsorb *via* formation of a donor bond between the O atom and a threefold-coordinated tetrahedral Al [Al(T_d)] surface site. The highest occupied molecular orbital (HOMO) of the free molecule is, in all cases, composed largely of non-bonding orbitals on the O atom of the P=O group. The empty "dangling orbital" on the coordinatively-unsaturated Al(T_d) site constitutes a surface state. A linear relationship is found between ΔE_{ads} and the difference between the orbital energies of the molecular HOMO (ε_H) and the surface state (ε_S). Trends in ΔE_{ads} for different molecules can then be understood in terms of variations in ε_H. Likewise, differences in ΔE_{ads} for various cluster models can be explained by considering the differences in the predicted ε_S values. A further evaluation of the cluster models is presented by comparing results for the physisorption of H₂O or CO with those obtained from two-dimensionally-periodic slab models. When differences in ε_H and ε_S are accounted for, the various models and computational procedures are seen to yield essentially equivalent results for adsorption of the molecules considered. These results are thought to constitute a useful conceptual tool for rationalizing ΔE_{ads} values for different molecules and cluster models.

Published by Elsevier B.V.

1. Introduction

Many highly toxic chemicals involve the phosphonyl (P=O) functional group. These include herbicides and pesticides as well as chemical warfare agents (CWAs) such as Tabun (GA), Sarin (GB), Soman (GD) and VX. The adsorption of these species on various substrates is an important issue in "agent fate", i.e., the stability of the adsorbate with respect to desorption, decomposition and reaction with environmental species. In both experiment [1,2] and theory [3–6], adsorption on the surface of a Lewis-acid material such as OH-free γ-Al₂O₃ occurs *via* dative bond formation involving the phosphonyl O atom and a coordinatively-unsaturated cation surface site. Non-bonding orbitals (NBOs) on the former comprise the highest-occupied molecular orbital (HOMO) of the free molecule. Unoccupied orbitals localized mainly on the surface cations form a band of surface states on the oxide.

One purpose of this work is to explore the correlation between the adsorption energy (ΔE_{ads}) and the energy of the HOMO relative to that of the surface state. This involves the "frontier orbitals" concept of chemical bonding [7–9] which, to our knowledge, has not previously been applied to a quantitative description of adsorption in these systems. The molecules studied (Fig. 1) were chosen to exhibit a fairly wide range of ionization potentials (IPs, see below).

These include trichlorophosphine oxide (TCPO), dimethyl methylphosphonate (DMMP), Sarin and trimethylphosphine oxide (TMPO). They were also chosen to be fairly small so that steric effects would not seriously complicate the interpretation of ΔE_{ads}. DMMP is also of interest since it is frequently used as a safe simulant for Sarin. Another purpose is to understand how the choice of cluster model affects the final results for the adsorption of these species. This study involves several issues and computational approaches. The properties of the free molecules, the surface-state structure of the bare semi-infinite γ-AlO₃ surface and of different cluster models and the interaction of the molecules with the clusters all have to be considered in unison.

2. Computational details

2.1. Molecular properties

The free molecules, and also various clusters designed to model the reactive site on the γ-Al₂O₃ surface, were treated using density functional theory (DFT) as implemented in the Gaussian 03 [10] and the *Amsterdam density functional* (ADF) *2006.01* [11] suites of programs. The former calculations employed the B3LYP hybrid functional with 6-311G(d) basis sets, "tight" convergence criteria in geometry optimization and an "ultrafine" integration grid. The *ADF* calculations used the Vosko–Wilk–Nusair (VWN) form of the local density approximation (LDA) and the Perdew–Burke–Ernzerhoff

* Tel.: +1 202 767 6728; fax: +1 202 767 1165.
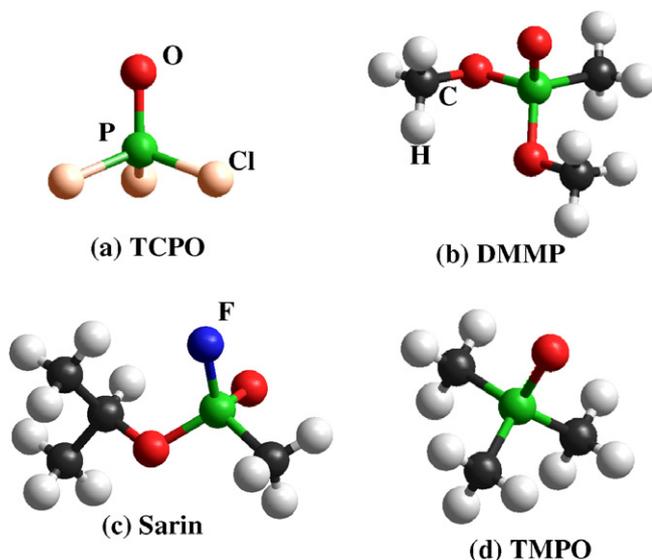*E-mail address:* victor.bermudez@nrl.navy.mil.

Fig. 1. Molecular structures for TCPO, DMMP, Sarin and TMPO. The Sarin enantiomer was arbitrarily chosen.

(PBE) form of the generalized gradient approximation (GGA) exchange-correlation (XC) potential. The *ADF* basis sets, designated "TZP", were Slater-type functions of triple-zeta quality with a single p polarization shell for H and a single d polarization shell for all other atoms. These are all-electron basis sets with no "frozen cores" (cf. Ref. [11]). The criteria for integration accuracy and geometry convergence (10^{-6} Hartree total energy; 1×10^{-3} Hartree/Å gradient; 1×10^{-3} Å displacement) were tighter than the *ADF* defaults (in order to facilitate the computation of vibrational frequencies) but looser than those used in the Gaussian calculations.

Vertical ionization potentials (VIPs) were calculated using the Δ(SCF) method [12]. Here the ground-state geometry is optimized and the total energy obtained. Then an electron is removed from the HOMO and the total energy computed, in a spin-unrestricted calculation, with the nuclei fixed in the ground-state positions. The energy difference is the VIP which can be compared with data from photoelectron spectroscopy (PES). Adiabatic ionization potentials (AIPs) were obtained similarly except that the cation geometry was allowed to relax. The AIP difference in energies was adjusted for the difference in the total vibrational zero-point energy (ZPE) which amounts to a correction of $\leqslant 70$ meV for the present molecules. Stability tests [13] were performed for the B3LYP calculations and the cation wavefunction was reoptimized in one case (TMPO) where an instability was found (see below). For B3LYP/6-311G(d) calculations, the harmonic vibrational frequencies were scaled by a factor of 0.9669 following results [14] for B3LYP/6-311G(d,p). No correction was applied for the (VWN + PBE)/TZP calculations since the scaling factor in this case is estimated [14] to be close to unity.

2.2. Bulk and two-dimensionally-periodic slab models for γ-Al$_2$O$_3$

Calculations for bulk γ-Al$_2$O$_3$ and for a two-dimensionally periodic slab (2-DPS) were done using the Crystal 03 suite of programs [15,16] in order to study surface states. The B3LYP hybrid functional was used due to its demonstrated [17] ability to give band gaps in good agreement with experiment for a wide range of materials including Al$_2$O$_3$. All-electron Gaussian basis sets [15] for Al and O, designated 86-21d1G (or 86-21G(d)) and 8-411d11G (or 8-411G(2d)), respectively, were used without modification to construct Bloch functions. The *k*-point sampling used an $8 \times 8 \times 8$ ($8 \times 8 \times 1$) grid for the bulk (2-DPS) and an "extra-large"

(75,974) DFT integration grid. In Crystal, truncation of the sums of Coulomb and exchange terms in the Fock matrix is determined by five overlap criteria (T1–T5) [15,16]. These were set at 10^{-7} for T1–T4 and 10^{-14} for T5. In the multipolar expansion zone [15,16] a maximum order of L = 6 was used.

The γ-Al$_2$O$_3$ model used here is the defective-spinel structure given by Pinto et al. [18] on the basis of plane-wave pseudopotential LDA calculations. The bulk- (and thus the surface-) structure of γ-Al$_2$O$_3$ is a subject of controversy [18–29], the essential aspects of which are summarized elsewhere [30–32]. Realistic models of high-surface-area γ-Al$_2$O$_3$ powders, even in the absence of hydroxylation, may involve a wide variety of different Al and O surface sites as discussed in, for example, Ref. [33]. The choice of bulk model and surface plane determines the distribution and identity of potential reactive sites. For example, the (1 0 0) surface of the non-spinel model [22] exposes three inequivalent fivefold-coordinated Al(O$_h$) sites, each with a different chemical character. The present work focuses on one particular type of surface site; namely, the threefold-coordinated Al(T$_d$). This is most easily modeled (see below) using the (1 1 1)a surface of the defective-spinel structure [18] but also occurs on the (1 1 0) surface of the non-spinel model [22]. Hence, the present work is primarily a study of adsorption at threefold-coordinated Al(T$_d$) sites rather than on a particular surface plane of a specific bulk-lattice model. It will be shown below that the essential difference among these models lies in the energies of the empty surface states derived from cations.

In the present work, the lattice constants were kept fixed at the optimized bulk values [18] while the atom positions were allowed to vary in a geometry optimization of the bulk structure. Only very small differences (<0.002) were found between the fractional atom positions and those of the initial structure [18]. A (1×1) slab unit cell was used with a thickness of 31 atomic layers (equivalent to one crystallographic unit cell) and the (1 1 1)a plane as the surface layer. The slab unit cell was symmetric about the mid-plane so that no dipole potential was generated. The (1 1 1)a, which has been identified [18] as the most stable surface of a bulk single crystal, consists of singly-unsaturated tetrahedral Al(T$_d$) sites and two types of O sites. One is threefold-coordinated in the bulk, as a result of being adjacent to a vacant octahedral Al(O$_h$) spinel site, and remains so at the surface. This O has one Al(T$_d$) and two Al(O$_h$) nearest-neighbors. The other O is fourfold-coordinated in the bulk but is missing its Al(T$_d$) nearest-neighbor at the surface. The Al(T$_d$) is a strong Lewis-acid site on the γ-Al$_2$O$_3$ surface [22,34], and there are no unsaturated Al(O$_h$) sites on the (1 1 1)a surface. Upon relaxing the slab, with the lattice constants fixed but all atoms unconstrained, it was found that the atomic displacements were small (<0.1 Å) beyond the outermost few planes, in agreement with previous results [18].

2.3. Cluster models for γ-Al$_2$O$_3$

Three different cluster models (Fig. 2) were used, all of which are described in detail elsewhere [3,4]. All are derived from the (1 1 1)a defective-spinel surface discussed above. One is an Al$_{20}$O$_{30}$ structure with unsaturated edge atoms [3], and the others are Al$_8$O$_{12}$ and Al$_{32}$O$_{48}$ clusters with pseudo-hydrogen termination (PHT) [4,35]. A pseudo-hydrogen (PH) is a neutral atom with a non-integer nuclear charge and electron occupancy. Each PH supplies to a coordinatively-unsaturated Al or O the amount of charge that would be derived from the missing nearest-neighbor in the γ-Al$_2$O$_3$ lattice. Due to the presence of both four and sixfold-coordinated Al atoms, four different PHs are needed which are shown in Fig. 2b as H$_{1/2}$, etc. An H$_{1/2}$, for example, has a nuclear charge of +1/2 |e| and an electron occupancy of −1/2 |e|. H$_{1/2}$ and H$_{3/4}$ are used to terminate O atoms, and H$_{5/4}$ and H$_{3/2}$ are used to
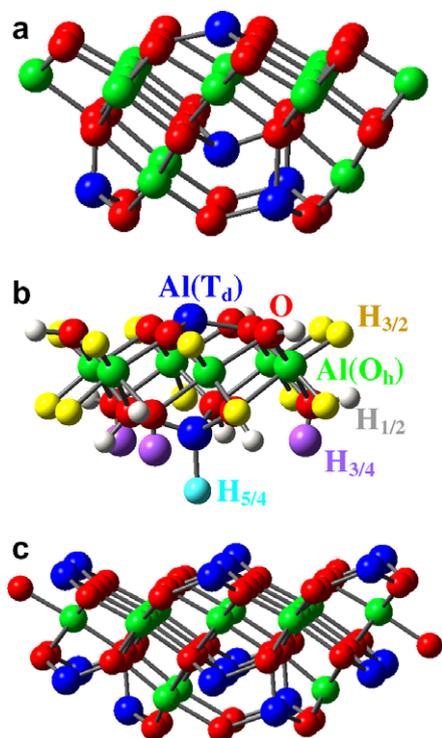
Fig. 2. Cluster models used in this study. (a) $Al_{20}O_{30}$ with unsaturated edge atoms, (b) Al_8O_{12} with PHT, (c) $Al_{32}O_{48}$ with PHT. For clarity the $Al_{32}O_{48}$ pseudo-Hs are not shown, and different scales have been used for the various structures. $H_{1/2}$, etc. are pseudo-Hs.

terminate Al atoms. For clarity the PHs in the $Al_{32}O_{48}$ model have been omitted from Fig. 2c.

The adsorption energy, corrected for basis set superposition error (BSSE), is defined as

$$\Delta E_{ads} = E(\text{cluster} + \text{mol}) - E(\text{cluster}) - E(\text{mol}) + \Delta E(\text{BSSE})$$

where the Es are, respectively, the relaxed total energies of the cluster with the adsorbed molecule, of the bare cluster and of the free molecule. The last term is the counterpoise correction for BSSE. A negative ΔE_{ads} indicates an exothermic adsorption process. Calculations for the clusters with PHT were done using *ADF* (which permits the use of PHs) and the TZP basis sets described above. For technical reasons these were done using the (VWN + PBE), rather than the B3LYP, functional. For continuity with previous work [3], calcula-

tions for the $Al_{20}O_{30}$ cluster (without PHT) were done using Gaussian 03 and the B3LYP functional. This model may be viewed as an Al_8O_{12} sub-cluster situated within a larger cluster. The molecule and the Al(–O–)$_3$ adsorption site were modeled with 6-311G(d) basis sets, while 6-31G(d) basis sets were used for the rest of the Al_8O_{12} sub-cluster. Atoms outside the sub-cluster were modeled with 3-21G basis sets. The $Al_{20}O_{30}$ ΔE_{ads} results obtained here for Sarin and DMMP (see below) differed by <1 kcal/mol from previous results [3] obtained using 6-311G(df) basis sets for the molecule and the Al(–O–)$_3$ site. The $Al_{20}O_{30}$ results showed both internal and spin-restricted/spin-unrestricted instabilities [13] due to the unsaturated edge atoms. Reoptimizing the wavefunction to eliminate these instabilities lowered the total energy (with or without adsorbates) by about 3 kcal/mol. In computing ΔE_{ads} this effect approximately cancelled, leading to a net reduction in adsorption energy of only ∼0.4 kcal/mol relative to the uncorrected result.

Geometry optimization began, for the bare clusters, with relaxing the positions of the Al(–O–)$_3$ adsorption site and of the PHs (if present) while keeping all other Al and O atoms fixed in the ideal-lattice positions. For adsorption the PHs remained fixed in the optimized positions while atoms in the molecule and in the Al(–O–)$_3$ adsorption site were allowed to vary. Optimizations involving Al_8O_{12} were done using the same convergence criteria as for the free molecules (see above). For $Al_{32}O_{48}$ the convergence criteria were relaxed to the *ADF* defaults. For consistency in obtaining ΔE_{ads} the same criteria were used for all three components (adsorbate + cluster, bare cluster and free molecule).

Vibrational normal modes were also obtained for adsorbates on the $Al_{20}O_{30}$ and Al_8O_{12} (PHT) clusters. Due to the large number of atoms involved this was not attempted for the $Al_{32}O_{48}$ (PHT) cluster. The interest here is in the internal modes of the molecule, particularly in ν(P=O), the frequency of the P=O stretching vibration. These receive little or no contribution from displacements of atoms in the cluster itself (including the PHs). Hence, the results are considered to be reliable even though only partial geometry optimizations are performed, as noted above.

3. Results

3.1. Free-molecule structures, vibrational frequencies and ionization potentials

Table 1 shows computed structural parameters for the free molecules together with data for TCPO from microwave (μ-wave) spectroscopy [36] and for TMPO from X-ray crystallography [37]. To our knowledge, no corresponding structural parameters are available

Table 1
Observed and calculated structural and vibrational parameters for free molecules[a]

	r(P=O)	r(P–X)	∠(O=P–X)	∠(X–P–X)	ν(P=O)[b]
TCPO[c]	*1.455*	*1.989*	[d]	*103.7*	*1321*
	1.462 (1.474)	2.042 (2.030)	114.9 (114.6)	103.5 (103.9)	1268 (1274)
Sarin					*1311*
	1.473 (1.481)				1256 (1260)
DMMP					*1276*
	1.482 (1.490)				1223 (1230)
TMPO[e]	*1.489*	*1.771*	*112.8*	*105.9*	*1148*
	1.498 (1.503)	1.830 (1.829)	114.1 (113.9)	104.4 (104.7)	1178 (1193)

[a] Observed values are italicized. Non-italicized values are computed. The first value is at the B3LYP/6-311G(d) level, and the value in parentheses is at the (VWN + PBE/TZP) level. X ≡ Cl for TCPO and CH$_3$ for TMPO. Bond lengths are in Ångstroms, and bond angles are in degrees. No experimental structural parameters are available for DMMP or Sarin.

[b] ν(P=O) is in cm^{-1}. The experimental values for TCPO [43], DMMP [44] and Sarin are from gas phase infrared spectra. The TMPO value is for the solid [45]. The Sarin value is an estimate [3] based on data for the liquid [2]. Calculated values all pertain to the gas phase.

[c] Experimental structural parameters are from Ref. [36].

[d] No experimental value is given.

[e] Experimental structural parameters are given in Ref. [37]. In the crystal one C atom lies in a mirror plane together with the P=O group and is, therefore, inequivalent to the other C atoms which lie above or below the plane. This slight inequivalence is ignored in the table, and the experimental values given are averages over all CH$_3$ groups.

Table 2
Calculated HOMO energies (ε_H) and ionization potentials (eV) for free molecules[a]

	TCPO	Sarin	DMMP	TMPO
HOMO energy (ε_H)	9.51 (8.04)	8.30 (6.98)	7.82 (6.53)	7.19 (5.93)
Calculated (vertical IP)	11.77 (11.06)	10.60 (10.17)	10.17 (9.80)	9.62 (9.53)
Calculated (adiabatic IP)	11.25 (10.82)	9.90 (9.60)	9.47 (9.29)	9.10 (9.12)
Experimental (vertical IP)	11.89[b]	11.14[c]	10.71[b]	9.88[d]

[a] Values not in parentheses are calculated at the B3LYP/6-311G(d) level. Values in parentheses are calculated at the (VWN + PBE)/TZP level.
[b] From PES data, Ref. [46].
[c] No experimental value is available. For Sarin, a VIP of 11.14 eV is estimated (see text) based on the DMMP results.
[d] From PES data, Ref. [47].

for either DMMP or Sarin; although, moments of inertia are available from μ-wave data [38,39]. Generally good agreement is seen between the two different calculations and between observed and calculated values for TCPO and TMPO.

Sarin and DMMP exhibit different conformers which have been studied using μ-wave spectroscopy and *ab initio* or semi-empirical theory [38–42]. In the present work the free molecules, upon geometry optimization, relaxed into the lowest-energy conformations as reported previously [38–40] and shown in Fig. 1. For Sarin, calculations of the relaxed total energy *vs.* the angle of rotation of the $(CH_3)_2(H)C–$ group about the C–OP bond were done in 10° steps at both the (WWN + PBE)/TZP and B3LYP/6-311G(d) levels. The results (not shown) were very similar to those obtained previously [40] at the B3LYP/6-31G(d,p) level.

Table 1 also shows observed and calculated values for $v(P{=}O)$, which is sensitive to adsorption (see below). The experimental values for TCPO [43], DMMP [44] and Sarin (an estimate [3] based on data for the liquid [2]) are all for the gas phase and can be compared directly with the computed results. On the other hand TMPO is a solid, and infrared data were obtained for a powder dispersed in mineral oil [45]. $v(P{=}O)$ is known to be significantly red-shifted in the condensed phase due to intermolecular interactions, which are not included in the calculation. For example, $v(P{=}O)$ is 31 cm^{-1} lower in liquid *vs.* gas-phase DMMP [44]. Except for solid TMPO, the experimental results are consistently 51 ± 4 cm^{-1} higher than the calculated values. This suggests a systematic error in the calculation which should cancel, approximately, in obtaining $\Delta v(P{=}O)$, the shift caused by adsorption. It was also found that $v(P{=}O)$ for free Sarin is essentially independent of conformation. At the B3LYP/6-311^{++}G(d,p) level a difference of only about 4 cm^{-1} was found between the lowest-energy ("Sarin-I") and highest-energy ("Sarin-III") conformations as defined in Ref. [40].

The orbital energies of the molecular HOMOs are needed in the following discussion. Since these bear some relation to experimentally-observable IPs these quantities have been computed for the free molecules. Table 2 shows the VIP and AIP results, together with the HOMO orbital energies for the neutral species. The VIPs can be compared directly with PES data [46,47] which show better agreement in the case of B3LYP/6-311G(d). For B3LYP the largest discrepancy between experiment and calculation (0.54 eV) is for DMMP, which is chemically similar to Sarin. Correcting the computed VIP for Sarin (10.60 eV) by this amount leads to an estimate of about 11.14 eV for the actual VIP.

For TCPO and TMPO the HOMO is twofold degenerate, with large contributions from p_x and p_y NBOs on the O atom of the P=O group (which is aligned along the z-axis). For Sarin and DMMP the degeneracy is lifted with splittings of about 0.05 and 0.09 eV, respectively, between the HOMO and HOMO-1. This effect is neglected in Table 2 which gives IPs derived from ionization of the HOMO. All quantities show the same trend, decreasing in magnitude monotonically in the order TCPO > Sarin > DMMP > TMPO. This reflects the inductive effect of strongly- *vs.* weakly-electronegative species (e.g., Cl *vs.* CH$_3$) on the P atom and, in turn, on the

HOMO energy. It is noted in passing that, in computing the AIP, a Jahn–Teller distortion (which breaks the C_{3v} symmetry) was found for the TCPO and TMPO cations. Further discussion of this aspect is beyond the scope of the present work.

3.2. γ-Al$_2$O$_3$ Al(T_d) surface state

Empty surface states can be identified using electron energy loss spectroscopy (ELS). As in optical absorption, the transition energy includes the effect of electron–hole interaction and thus provides only a lower limit on the separation between the initial and final levels in the electronic ground state. Inverse photoemission spectroscopy [48] or tunneling spectroscopy can also be used to study empty surface states, without the perturbing effects of core or valence holes, but such data are not to our knowledge available for γ-Al$_2$O$_3$.

One ELS experiment was reported [49] for a (111)-oriented γ-Al$_2$O$_3$ film grown by thermal oxidation of a NiAl (110) surface. No surface states were seen in the band gap. However, the (111) surface in this case is believed [50] to be O-terminated and, hence, would not be expected to show empty Al-derived surface states. Ultra-thin γ-Al$_2$O$_3$ films have been formed by oxidation of a Ni$_3$Al(100) surface [51]. These show a band gap of $E_g \approx 4.3$ eV, much smaller than that for defect-free bulk γ-Al$_2$O$_3$ ($E_g = 7.2$ eV [52]). This was ascribed to the presence of defects, and in any case, such ultra-thin oxide films may not be representative of the bulk material [53]. Thus the experimental situation regarding empty surface states on γ-Al$_2$O$_3$ is uncertain at present.

A theoretical study has been performed [18] for various γ-Al$_2$O$_3$ surfaces using plane-wave pseudopotentials and a 2-DPS model based on the defective-spinel structure. The computed bulk band gap ($E_g = 3.97$ eV) underestimates the experimental value, as is typical in LDA calculations [54]. On the (111)a surface the valence band maximum (VBM) is found to move down, and the conduction band minimum (CBM) to move up, relative to the respective bulk band edges which leads to a surface band gap of about 4.7 eV. On this surface, a narrow band of states derived from empty Al(T_d) orbitals is found at about 1.3 eV below the surface CBM. Similar calculations have been done for the (100) and (110) surfaces of the non-spinel structure [22]. These also show distinct surface-state features near the CBM which are assignable to each of the different unsaturated Al sites.

To obtain an independent assessment of the surface-state energy, calculations were performed for the bulk lattice and for the 2-DPS as described above. For the bulk lattice an E_g of 6.2 eV was found which is in fair agreement with experiment ($E_g = 7.2$ eV [52]). A previous B3LYP treatment for an unspecified form of Al$_2$O$_3$ (presumably α-Al$_2$O$_3$) gave a bulk E_g of 8.5 eV [17] *vs.* the experimental α-Al$_2$O$_3$ value of 8.8 eV [52]. Fig. 3 shows the density of states for the 2-DPS in the vicinity of the band edges. A surface E_g of about 7.0 eV is found with the lowest-energy surface-state (S1) located just below (within ~0.5 eV from) the CBM. A second surface state (S2), also derived from surface Al(T_d) sites, is found at
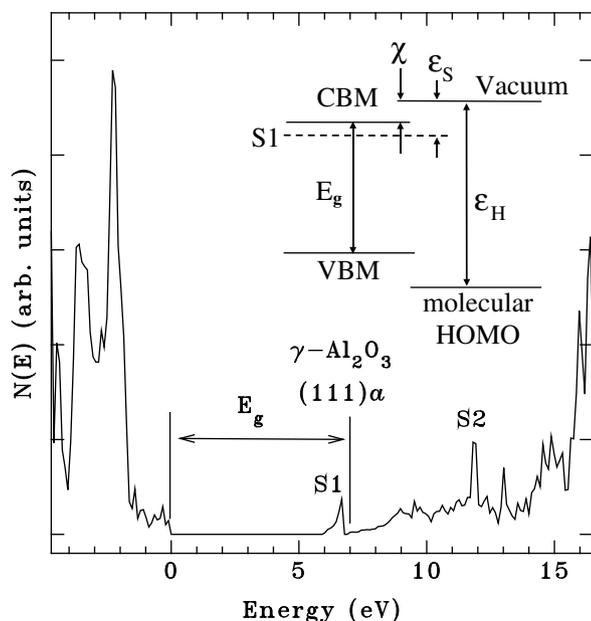
Fig. 3. Density of states, in the vicinity of the band edges, computed in the present work for the 2-DPS model of γ-Al_2O_3. The bulk band gap and the positions of the empty surface states (S1 and S2) are indicated. The zero of energy is at the VBM. The inset shows a schematic energy level diagram (not to scale) with definitions of various quantities.

about 4.8 eV above the CBM. The larger E_g for the slab *vs.* the bulk lattice is consistent with previous results [18]. The position of S1 is essentially in agreement with that given previously [18]; although, the present work finds it lying somewhat closer to the CBM.

It now remains to be seen how closely the various cluster models reproduce the 2-DPS S1 position. The Al_8O_{12} cluster (with PHT) gives a "band gap" of about 4.4 eV. This is taken as the energy difference between the HOMO and the lowest-energy virtual state not receiving any substantial contribution from atomic orbitals localized on the unsaturated $Al(T_d)$ "surface" cation. The "surface state" associated with this site then falls at about 1.0 eV below the "CBM". Similar results were found [35] for an Al_8O_{12} cluster with PHT designed to model the α-Al_2O_3 (0001) surface. The PHs in this case are different from those used for γ-Al_2O_3 since all Al sites in α-Al_2O_3 are $Al(O_h)$, and there are no cation vacancies. For this model [35], after relaxation, $E_g \approx 4.5$ eV was found with the surface state at about 0.5 eV below the "CBM". The surface state in this case arises from the threefold-coordinated $Al(O_h)$.

The $Al_{32}O_{48}$ cluster (with PHT) gave $E_g = 4.3$ eV with the surface state at about 0.6 eV below the CBM. As shown in Fig. 2c, the "surface" of this cluster comprises seven $Al(T_d)$ sites. The central Al, which is the adsorption site in the model calculation, is different from the others in that it is threefold-coordinated to O atoms. The other such Al sites are all bonded to a PH (not shown in Fig. 2c) to compensate for a missing Al–O back-bond. The S1 state is taken as the virtual state in the gap which is composed largely of atomic orbitals associated with this central atom. Other such gap states, derived from orbitals centered on the peripheral $Al(T_d)$ sites, lie higher in energy and are not involved in chemisorption (see below). On the (1 1 1)a surface of the 2-DPS all Al sites are equivalent to the central $Al(T_d)$.

For the $Al_{20}O_{30}$ cluster (without PHT) there are many states in the "band gap" due to the unsaturated Al and O atoms at the periphery of the cluster. The "bulk VBM" was determined by identifying the highest occupied molecular orbital with large contributions from fully-coordinated O atoms. Likewise the "bulk CBM" was identified by finding the lowest virtual orbital with large con-

tributions from fully-coordinated Al atoms. The result is $E_g \approx 5.8$ eV with the $Al(T_d)$ surface state at ~0.2 eV below the CBM. Hence, all three cluster models predict approximately the correct location for S1 relative to the CBM in comparison to the B3LYP 2-DPS result.

The question of occupied surface states derived from O atoms has also been considered. For the (1 1 1)a surface none are predicted in 2-DPS calculations to occur above the bulk VBM, either here or in previous work [18], and none are observed experimentally in ultraviolet photoemission spectroscopy data [50,55]. For the $Al_{32}O_{48}$ PHT cluster, however, states within ~1 eV of the VBM are derived largely from surface O atoms (i.e., those in the uppermost O layer). This affects the estimates of E_g given above but not the central issue, which is the position of S1 relative to the CBM.

3.3. Energy level alignment

It is now necessary to define a common reference for the energy levels of the cluster and the molecule. Formation of the dative bond (see below) involves the transfer of only a small amount of charge (~0.1–0.2|e|) from the P=O group to S1. Hence, it is meaningful to consider the chemical potential of an electron in the HOMO or in S1. Janak [56] has shown that $\varepsilon_i = \partial E/\partial n_i$ where ε_i is the DFT energy of orbital (i) and n_i is the orbital population (treated as a continuous variable in DFT). For a non-metallic system, in which many-body screening effects can be neglected, E is effectively the total energy. Therefore in the following discussion ε_H, the DFT orbital energy of the free-molecule HOMO, is taken as the chemical potential of an electron in the HOMO. Likewise ε_S, the DFT orbital energy of S1, is taken as the chemical potential of an electron in the surface state. The resulting ε_H and ε_S values are summarized in Table 3 and shown schematically in Fig. 3.

An electron affinity of $\chi \approx 1$ eV, which places the CBM relative to vacuum (cf. Fig. 3), has been estimated [57] for α-Al_2O_3. A χ of 1.35 eV has been estimated [58] for γ-Al_2O_3 on the basis of electron tunneling measurements [59] on an ultra-thin film on NiAl(1 1 0) [50]. As noted above, such films may not be characteristic of the bulk material. If one assumes, nevertheless, that χ is slightly larger than 1 eV for γ-Al_2O_3 and places S1 within ~0.5 eV of the CBM, as found in the present 2-DPS results, then $\varepsilon_s \approx 1.5$ eV is obtained as an estimate for the actual value. This is close to the $Al_{32}O_{48}$ result of 1.40 eV. Hence one expects, *a priori*, that the $Al_{32}O_{48}$ cluster will provide the most accurate model of the active site on the defective-spinel (1 1 1)a surface, a view which will be supported by results given below.

Table 3
Calculated ΔE_{ads} for different molecules and γ-Al_2O_3 model clusters[a]

	$Al_{20}O_{30}$[b]	ε_H[c]	Al_8O_{12}[d]	$Al_{32}O_{48}$[d]	ε_H[e]
TCPO	−33.3	9.51	−33.0	−24.7	8.04
Sarin	−49.0	8.30	−51.5	−39.8	6.98
DMMP	−57.2	7.82	−53.0	−41.4	6.53
TMPO	−62.2	7.19	−58.6	−51.2	5.93
ε_S[f]	4.01		2.18	1.40	

[a] All energies are kcal/mol and have been corrected for BSSE. BSSEs computed for Al_8O_{12} was also used for $Al_{32}O_{48}$ since the adsorption geometry and computational conditions are essentially the same in both cases.
[b] Results for $Al_{20}O_{30}$ (no PH termination) obtained at the B3LYP/6-311G(d) level and corrected for the effects of wavefunction instabilities (see text).
[c] HOMO orbital energies calculated at the B3LYP/6-311G(d) level, from Table 2.
[d] Results for Al_8O_{12} and $Al_{32}O_{48}$ (both PH-terminated) obtained at the (VWN + PBE)/TZP level.
[e] HOMO orbital energies calculated at the (VWN + PBE)/TZP level, from Table 2.
[f] Surface state (S1) orbital energy determined as described in the text. A positive value indicates that S1 lies below the vacuum level.

3.4. Adsorption energies, geometries and vibrational frequencies

The main theme of this work is the dependence of ΔE_{ads} on ε_H and ε_S. The essential results are summarized in Table 3. Fig. 4a shows, as an example, the optimized structure of TMPO adsorbed on the Al_8O_{12} cluster (with the PHs removed for clarity). For other adsorbates the structure is similar in appearance (e.g., Ref. [3]). For a given cluster, comparing results for different molecules shows the correlation between ΔE_{ads} and ε_H. As one expects intuitively on the basis of the frontier-orbital concept [7–9], decreasing ε_H makes charge transfer easier and leads to an increased ΔE_{ads}. For a given molecule, comparing results for the Al_8O_{12} vs. $Al_{32}O_{48}$ clusters shows the correlation between ΔE_{ads} and ε_S. Again as expected, moving S1 up toward vacuum makes the surface less acidic (i.e., a weaker acceptor) and impedes dative-bond formation, thus decreasing the magnitude of ΔE_{ads}.

Fig. 5 shows plots of the results in Table 3. All clusters yield an essentially linear dependence of ΔE_{ads} on $(\varepsilon_H - \varepsilon_S)$ with slightly different parameters for $Al_{20}O_{30}$ vs. Al_8O_{12} and $Al_{32}O_{48}$. Initially the Al_8O_{12} and $Al_{32}O_{48}$ results were fitted separately, but the fits were virtually indistinguishable and Fig. 5 shows a single fit for both. The reason for the small differences between the PHT and non-PHT parameters (about 5% in the slope and 2% in the intercept) is difficult to identify. One possibility is the different DFT functionals used for the two sets of calculations.

Although the qualitative dependence of ΔE_{ads} on ε_H and ε_S is expected, the quantitatively linear behavior in Fig. 5 is not. A linear combination of atomic orbitals (LCAO) treatment (e.g., Refs. [7,9]) yields $\Delta E_{ads} = H^2/\Delta\varepsilon$ where H is the interaction energy between the empty S1 state and the doubly-occupied molecular HOMO and $\Delta\varepsilon = \varepsilon_S - \varepsilon_H$. This is based on a perturbation approximation ($|H| \ll |\Delta\varepsilon|$) which does not apply in the present case since, for the ΔE_{ads} and $\Delta\varepsilon$ values encountered here, H and $\Delta\varepsilon$ would be of
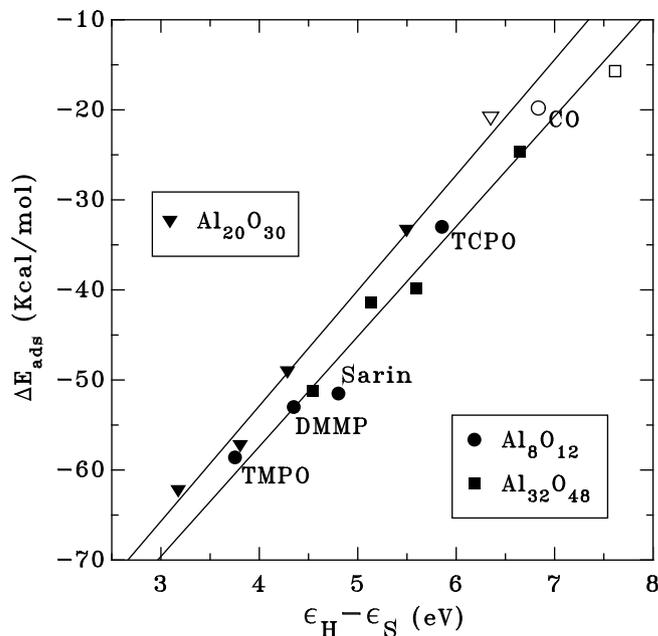
Fig. 5. Graphical display of the results in Table 3. The linear regressions are given by $\Delta E_{ads} = -106.2 + 12.22(\varepsilon_H - \varepsilon_S)$ for Al_8O_{12} (circles) and $Al_{32}O_{48}$ (squares), $r = 0.984$ $\Delta E_{ads} = -104.1 + 12.82(\varepsilon_H - \varepsilon_S)$ for $Al_{20}O_{30}$ (triangles), $r = 0.995$ with ΔE_{ads} in kcal/mol and $(\varepsilon_H - \varepsilon_S)$ in eV. The r values are the correlation coefficients. Data points are labeled for Al_8O_{12} and appear in the same order for the other plots. The open symbols show ΔE_{ads} values computed for CO (see text) which were not included in the linear regression analysis.

similar magnitude. Fits to ΔE_{ads} which were linear in $1/\Delta\varepsilon$ (not shown) were not quite as good as those in Fig. 5. Different fits were obtained for Al_8O_{12} and $Al_{32}O_{48}$ when plotting vs. $1/\Delta\varepsilon$, with correlation coefficients of $r = 0.931$, 0.967 and 0.981 for Al_8O_{12}, $Al_{20}O_{30}$ and $Al_{32}O_{48}$, respectively.

When the effects of ε_H and ε_S are "factored out", similar behavior is seen for different cluster models, functionals and basis sets. With all else equal, differences in ΔE_{ads} for various clusters can be traced primarily to differences in ε_S. Previous 2-DPS results for γ-AlO_3 [22], obtained for the non-spinel bulk structure, have shown that the Lewis acidities of the various types of Al surface sites can be correlated directly with the energies of the corresponding empty surface states relative to vacuum (ε_S in the present notation). Energies in the range of $-2.5 \leqslant \varepsilon_S \leqslant +0.1$ eV were reported (using a sign convention opposite to that used here). In particular, $\varepsilon_S = -2.5$ eV was found for the threefold-coordinated $Al(T_d)$ site on the $(1\,1\,0)$ surface which is close to the value of $(-)2.18$ eV obtained here (Table 3) for the Al_8O_{12} (PHT) cluster. It was also found that the strength of the interaction of CO with these sites, as measured by ΔE_{ads} and by $\Delta v(C{=}O)$, correlates with the difference between ε_S and ε_H (the energy of the CO HOMO, i.e., the 5σ orbital). A further discussion of these points, including CO adsorption, is given below.

All adsorbates except TCPO show the possibility of H-bonding between H atoms in the alkyl group(s) and O atoms in the Al_2O_3 cluster. This is based on the observation, in the optimized structures, of one or more CH–O distances in the range of 2.1–2.4 Å. Similar effects have been noted in other studies [5,6] of CWA adsorption on ionic oxides. No attempt has been made here to assess the contribution of these effects to ΔE_{ads}. However, ab initio studies of other systems [60,61] suggest that such CH–O bonds are weak, with a bond energy of at most $\sim$3 kcal/mol.

Cluster models of the sort used here neglect the long-range contribution to the electrostatic potential at the adsorption site that would arise in a semi-infinite lattice. The possibility was considered that a difference in this potential could contribute to the dif-
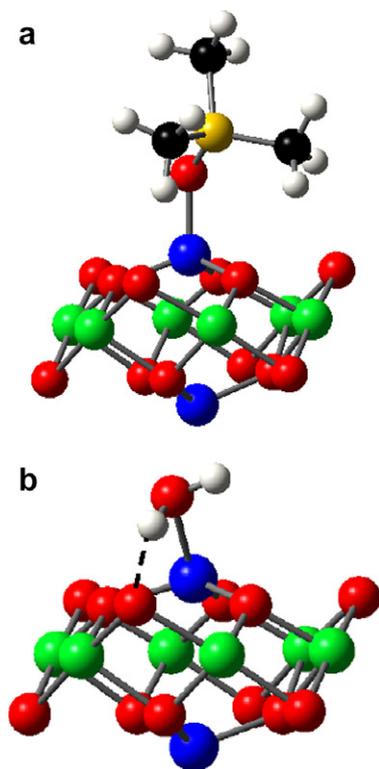

Fig. 4. Model showing the optimized structure for (a) TMPO and (b) H_2O adsorbed on the Al_8O_{12} cluster. The pseudo-Hs have been removed for clarity. In (b) the dashed line shows a hydrogen bond with $r(O–H) = 1.964$ Å.

ference in ΔE_{ads} for the various clusters. With the active Al(T$_d$) as the test site (j), the sum of q_i/r_{ij} over all other sites (i) including the PHs gave −1.232 and −1.173 |e|/Å for Al$_8$O$_{12}$ and Al$_{32}$O$_{48}$, respectively. Here q_i is the ionic charge computed using the multipole-derived charge (quadrupole), or MDC-Q, method of Swart et al. [62], and r_{ij} is the distance from (j). Likewise the MDC-Q charge on the active Al(T$_d$) site of the bare cluster is similar for Al$_8$O$_{12}$ (+1.82) vs. Al$_{32}$O$_{48}$ (+1.77). For comparison, a Mulliken charge of +1.66 is found for the surface Al(T$_d$) ion in the 2-DPS calculation described above. For the Al$_{20}$O$_{30}$ cluster, a Mulliken charge of +1.30 is found for the "surface" Al(T$_d$), which is smaller than the corresponding values given above. However, the sum over all q_i/r_{ij} is −1.231 |e|/Å, essentially the same as that found for the other clusters. Hence, the electrostatic environment in the vicinity of the adsorption site is similar for all three clusters; although, it may of course differ from that for a semi-infinite crystal.

Examination of the cluster orbitals shows that adsorption removes S1 from the gap. Bonding orbitals, with large components from the phosphonyl O atom and small contributions from the Al(T$_d$) adsorption site, appear a few eV below the "VBM". This is direct (theoretical) evidence for the involvement of S1 in the chemisorption process. The MDC-Q results for Al$_8$O$_{12}$ and Al$_{32}$O$_{48}$ show that the charge transferred to the Al atom is the range of −0.11 to −0.21 |e|, depending on the cluster and the adsorbate.

The configuration of adsorbed Sarin differs slightly from the lowest-energy Sarin-I structure [40] of the gas-phase molecule. For the Al$_{20}$O$_{30}$ cluster the isopropyl group rotates about the C–OP bond by about 27° in the direction of Sarin-II; whereas, for the PHT clusters the rotation is by about 13° in the direction of Sarin-III. For all models, Table 4 shows that r(Al–OP) decreases with increasing ΔE_{ads} as expected. All models yield about the same (Al–O=P) angle for a given molecule except for Sarin where a larger angle is found for Al$_{20}$O$_{30}$ (153°) vs. Al$_8$O$_{12}$ and Al$_{32}$O$_{48}$ (131°). This probably results from the different Sarin configurations, noted above, for Al$_{20}$O$_{30}$ vs. Al$_8$O$_{12}$ and Al$_{32}$O$_{48}$. The orientation of the isopropyl group for Sarin adsorbed on Al$_{20}$O$_{30}$ requires a larger (Al–O=P) angle to avoid steric interaction between one of the CH$_3$ groups and the cluster.

The computed Δv(P=O) values for Al$_{20}$O$_{30}$ and Al$_8$O$_{12}$ are in fairly good agreement with each other and (where available) with experimental data except, again, in the case of Sarin for which the Al$_8$O$_{12}$ result is too large vs. experiment (−66 cm^{-1} [2,3]). The explanation for this is uncertain at present. It may lie in the different Sarin conformations in the two models; however, as noted above, v(P=O) for free Sarin appears to be essentially independent

of conformation. For adsorbed DMMP the computed P=O stretch is strongly coupled to modes at 1161 and 1174 cm^{-1}, and v(P=O) is taken as the average of these values.

Results for the gas-phase molecules (Table 1) show the expected decrease in v(P=O) with decreasing bond strength (i.e., with increasing r(P=O)). Table 4 shows that r(P=O) is in all cases greater for the adsorbed vs. the gas phase, consistent with a weakening of the P=O bond. The increase in bond length is small, being in the range of δr(P=O) ≈0.03 to 0.06 Å, but there does appear to be a rough correlation between Δv(P=O) and δr(P=O). However, the correlation between Δv(P=O) and ΔE_{ads} is somewhat more tenuous, as is seen by comparing results for TCPO and TMPO. These show essentially identical Δv(P=O) values but ΔE_{ads} values differing by nearly a factor of two. Similar behavior was found previously [63] for the adsorption of TCPO and DMMP on amorphous silica via H-bonding between Si–OH groups and the phosphonyl O atom. A ΔE_{ads} of −10.4 (−20.0) kcal/mol was computed for TCPO (DMMP), but the experimental Δv(P=O) values are about −34 and −19 cm^{-1}, respectively. The reason for this behavior lies in a unique property of TCPO, whereby Cl orbitals are strongly mixed with both the HOMO and the P=O π orbital. For the other species studied here the HOMO consists almost entirely of orbitals on the O atom of the P=O group. For TCPO, the HOMO and the P=O π-bond are in effect coupled, and perturbation of the former by adsorption then leads to a disproportionately strong effect on the latter and a correspondingly large Δv(P=O). Hence, some caution must be applied when interpreting Δv(P=O) strictly in terms of the strength of the adsorption bond.

Finally, other possible modes of adsorption were considered, even though experimental data [1,2] for DMMP and Sarin clearly indicate Al–O=P dative bond formation as the energetically-favored process. Adsorption of Sarin on the Al$_8$O$_{12}$ cluster gave ΔE_{ads} of −26.2 or −31.0 kcal/mol, respectively, for bonding between Al and the F or the isopropoxy O atom. These have not been corrected for BSSE, and doing so would reduce the magnitudes by ~2 kcal/mol. These can be compared with the BSSE-corrected value of −51.5 kcal/mol (Table 3) for Al–O=P bonding. These results are consistent with previous results [3] for the Al$_{20}$O$_{30}$ cluster. Bonding of TCPO to Al$_8$O$_{12}$ via an Al–Cl–P bond was also tested. During relaxation the molecule moved away from the surface, and no bond formed. For TCPO a "reverse" dative bond was investigated, wherein an O atom on the Al$_2$O$_3$ surface acts as an electron donor and the P atom acts as an acceptor. This might, in principle, be energetically feasible since the lowest unoccupied molecular orbital of gas-phase TCPO is computed to lie at 3.485 eV below vacuum

Table 4
Results for adsorption on γ-Al$_2$O$_3$ model clusters[a]

Cluster	Adsorbate	ΔE_{ads}	r(Al–OP)	r(AlO=P)[b]	∠(Al–O=P)	Δv(P=O)[c]
Al$_{20}$O$_{30}$	TCPO	−33.3	1.862	1.502 (1.462)	135	−113
	Sarin	−49.0	1.813	1.505 (1.473)	153	−56
	DMMP	−57.2	1.795	1.523 (1.482)	151	−79
	TMPO	−62.2	1.799	1.556 (1.498)	131	−114
Al$_8$O$_{12}$ (PHT)	TCPO	−33.0	1.887	1.506 (1.474)	133	−99
	Sarin	−51.5	1.838	1.521 (1.481)	132	−103
	DMMP	−53.0	1.819	1.523 (1.490)	149	−62
	TMPO	−58.6	1.815	1.549 (1.503)	129	−97
Al$_{32}$O$_{48}$ (PHT)	TCPO	−24.7	1.948	1.499 (1.474)	135	
	Sarin	−39.8	1.863	1.513 (1.481)	130	
	DMMP	−41.4	1.860	1.516 (1.490)	148	
	TMPO	−51.2	1.841	1.545 (1.503)	129	

[a] In all cases, adsorption is via Al–O=P dative bond formation (cf. Fig. 4). Energies are in kcal/mol, bond lengths in Ångstroms, bond angles in degrees and frequencies in cm^{-1}. The ΔE_{ads} values repeat those in Table 3.
[b] Numbers in parentheses are P=O bond lengths computed for the free molecules.
[c] Δv(P=O) is the calculated v(P=O) for the adsorbed species minus the calculated gas-phase value. No experimental Δv(P=O) data are available for TCPO or TMPO. For DMMP the experimental result is −60 cm^{-1} (Ref. [1]). For Sarin the estimated experimental result is −66 cm^{-1} (Refs. [2,3]).

at the (VWN + PBE)/TZP level. The molecule was initially positioned with P=O bond pointing away from the surface and with the three Cl atoms coplanar with the P atom. The $Al_{32}O_{48}$ cluster was used, and the P was positioned above a coordinatively-unsaturated O atom (see above). However, here again the molecule relaxed away from the surface with no bond formation.

3.5. Comparison of 2-DPS and cluster results

There are, to our knowledge, no experimental data giving ΔE_{ads} for the systems of interest here. It is therefore difficult to assess the absolute accuracy of the results. However, comparison can be made with results for a 2-DPS which is assumed to model the surface of a semi-infinite crystal more accurately than does a finite cluster. One such comparison is for the physisorption of molecular H_2O using the same functionals, basis sets, etc. as for the phosphonyl species. In all cases a dative bond (H_2O–Al) forms between the O atom and the unsaturated $Al(T_d)$ site. A 2-DPS result of −28.1 kcal/mol for the (1 1 1)a surface has been found by Pinto and Elliott [64] using a plane-wave pseudopotential approach. The results obtained here (corrected for BSSE) are ΔE_{ads} = −40.1, −36.5 and −30.8 kcal/mol, respectively, for the $Al_{20}O_{30}$, Al_8O_{12} (PHT) and $Al_{32}O_{48}$ (PHT) clusters. Again, ΔE_{ads} decreases in magnitude as ε_S shifts toward vacuum. The $Al_{32}O_{48}$ result is close to that found for the 2-DPS which suggests that this cluster, of the three used here, gives the most reliable absolute values for ΔE_{ads} in comparison to the (1 1 1)a defective-spinel surface.

In the case of H_2O adsorption there is evidence for a contribution to ΔE_{ads} from hydrogen bonding between H and surface O atoms. Fig. 4b shows, as an example, the optimized structure for the Al_8O_{12} (PHT) cluster which exhibits an H-bond with r(O–H) = 1.964 Å. This complicates somewhat an interpretation of ΔE_{ads} strictly in terms of dative-bond formation. Nevertheless, the trend in ΔE_{ads} vs. ε_S is in accord with that expected on the basis of the results for the phosphonyl species.

Another comparison can be made for the adsorption of CO, a weak Lewis base often used to probe the acidity of oxide surfaces. Adsorption occurs (e.g., Ref. [22]) via an Al–C≡O dative bond involving the 5σ orbital of CO which is the HOMO. A DFT calculation, as described above, was done for the (1 1 1)a-oriented 2-DPS using 6-311G(d) basis sets[1] for CO and a (1 × 1) surface unit cell with a CO at every surface $Al(T_d)$ site. The γ-Al_2O_3 slab was modeled using the same basis sets as those described above. It is assumed that any interaction between adjacent molecules can be neglected. Based on results [65] for CO adsorbed on MgO(1 0 0) and on the present intermolecular distance of 5.6 Å, lateral interaction is expected to decrease the magnitude of ΔE_{ads} by <0.5 kcal/mol relative to the value for an isolated molecule. CO was placed identically on both the upper and lower slab faces in order to maintain symmetry.

The 2-DPS calculation gave ΔE_{ads} = −10.1 kcal/mol with optimized bond lengths of r(Al–C) = 2.200 Å and r(C=O) = 1.122 Å. For the free molecule, r(C=O) = 1.127 Å was found using the same (B3LYP) functional and basis sets. The 5σ orbital has a slight antibonding character; hence, adsorption leads to a very small decrease in r(C=O). The $Al_{32}O_{48}$ PHT cluster gave a stronger interaction, with ΔE_{ads} = −15.7 kcal/mol, r(Al–C) = 2.144 Å and r(C=O) = 1.133 Å. The corresponding free-molecule r(C=O) was found to be 1.141 Å using the VWN + PBE functional and TZP basis sets. The Al_8O_{12} PHT cluster gave a still-larger ΔE_{ads} of −19.8 kcal/mol due to the lower-lying S1 (Table 3). Similar calculations for the $Al_{20}O_{30}$, as described above,

gave ΔE_{ads} = −20.8 kcal/mol with r(Al–C) = 2.136 Å and r(C=O) = 1.117 Å. All energies have been corrected for BSSE.

For free CO, an ε_H of 9.015 eV is found at the (VWN + PBE)/TZP level and 10.360 eV at the B3LYP/6-311G(d) level. With these results and the ε_S values given in Table 3, the calculated ΔE_{ads} values for CO can be placed in Fig. 5. In all cases the results are in good accord with extrapolations of the linear fits to the phosphonyl results. As was seen for H_2O, the $Al_{32}O_{48}$ result gives the best agreement with, but is larger than, the 2-DPS value of ΔE_{ads} = −10.1 kcal/mol for the (1 1 1)a defective-spinel surface. For comparison, 2-DPS calculations for CO adsorption at the $Al(T_d)$ site on the (1 1 0) surface of the non-spinel model give ΔE_{ads} = −18.2 [22] or −17.1 kcal/mol [33]. This site has a computed ε_S of 2.5 eV, as noted above. It is thus more acidic than the $Al(T_d)$ site on the $Al_{32}O_{48}$ cluster, with ε_S = 1.40 eV, but closer in acidity to that on the Al_8O_{12}, with ε_S = 2.18 eV. Thus the non-spinel values for ΔE_{ads} [22,33] are close to the Al_8O_{12} result of −19.8 kcal/mol.

4. Discussion

The present work analyzes a basic principle affecting dative-bond formation between phosphonyl reagents and Lewis acid sites on the γ-Al_2O_3 surface. Presumably the same considerations affect similar adsorption processes for other systems. Table 3 and Fig. 5 demonstrate the sensitivity of ΔE_{ads} to ε_H and to ε_S. In the absence of experimental data for ΔE_{ads} it is necessary to compare the cluster results with those for a 2-DPS. Such comparisons for H_2O and CO (see above) indicate that the $Al_{32}O_{48}$ PHT cluster at the (VWN + PBE)/TZP level gives the most accurate ΔE_{ads} in comparison to the 2-DPS model of the defective-spinel (1 1 1)a surface. Therefore by implication this model, of the three studied here, gives the most reliable representation of S1 for that surface. On the other hand, ε_S for the Al_8O_{12} PHT cluster is close to that found for the $Al(T_d)$ site on the (1 1 0) non-spinel surface. Consistent with this, the ΔE_{ads} values for CO adsorption are also found to be close for these two substrates.

It might appear that issues involved in the formulation of cluster models could be avoided simply by working exclusively with 2-DPS models. However, the molecules of interest here and in other CWA studies are comparable in size to, or larger than, the γ-Al_2O_3 (1 × 1) surface unit cell. Avoiding significant steric interaction between nearest-neighbor adsorbates in a 2-DPS calculation requires the use of a suitably large slab supercell which may make the calculation computationally intractable. Hence, clusters are still preferable (or even mandatory), provided that ε_S can be reliably obtained. Having constructed such a cluster model one can then proceed with some confidence that reasonable adsorption results will be computed.

It is worthwhile to re-examine previous work [3] in light of the present results. *Absolute* adsorption energies may be difficult to compute reliably for any model (cluster or 2-DPS) because of the need to reproduce the experimental ε_S which may itself be uncertain, as is the case here. However, other quantities of interest include the adsorption geometry (i.e., lengths and angles of the chemisorption bonds), shifts in adsorbate vibrational frequencies relative to the gas phase and, especially, *relative* adsorption energies for similar molecules or for different functional groups of the same molecule. These kinds of information can often be obtained even in calculations that are only qualitative with regard to the absolute ΔE_{ads}.

Consider, for example, ΔE_{ads} for the adsorption of DMMP *vs.* Sarin (Table 3). The $Al_{32}O_{48}$ results are in qualitative agreement with those obtained previously [3] for the much simpler $Al_{20}O_{30}$ model which show a larger ΔE_{ads} for DMMP. However, the difference of 1.6 kcal/mol is less than the previous estimate of

---

[1] The C and O basis sets were obtained from the Extensible Computational Chemistry Environment Basis Set Database, Version 02/02/06, developed and distributed by the Molecular Science Computing Facility; Environmental and Molecular Sciences Laboratory which is part of the Pacific Northwest Laboratory; P.O. Box 999; Richland, WA 99352; USA.

8.2 kcal/mol. The difference in ΔE_{ads} for the two molecules is now understood to result from the somewhat smaller ε_H of DMMP. Another example concerns adsorption *via* an Al bond to the phosphonyl *vs.* the alkoxy O atom of DMMP or Sarin. For Sarin at the B3LYP/6-311G(d) level, the simple $Al_{20}O_{30}$ cluster gives $\Delta E_{ads} = -30.9$ kcal/mol for bonding to the alkoxy O atom *vs.* -49.0 kcal/mol for bonding to the P=O, a difference of about 18 kcal/mol. A similar difference, -20.9 *vs.* -39.8 kcal/mol, is found at the (VWN + PBE)/TZP level for adsorption on the $Al_{32}O_{48}$ PHT cluster.

When considering the effects of different ligands on the relative adsorption energies of phosphonyl species it should be possible to use the easily-computed ε_H of the free molecule as a quantitative indicator. In view of the above discussion concerning H_2O adsorption, such use of ε_H involves an assumption that other forms of interaction, such as H-bonding, can be neglected. Likewise, in comparing relative adsorption energies for Lewis-acid sites on other oxides, insight can be obtained by computing (or measuring) ε_S. One assumes here that the substrate orbital involved in the adsorption corresponds to a well-defined surface state lying in the band gap and that any modification of the surface does not cause a significant change in the electronic structure of the surface state.

Similar considerations might apply even when the HOMO is not derived from NBOs on the P=O group. For example, other work [4] shows that adsorption of the nerve agent VX on OH-free γ-Al_2O_3 also involves Al–O=P bonding. However, the HOMO and HOMO-1 in this case are derived largely from NBOs on the nitrogen and sulfur atoms, respectively, neither of which is directly involved in chemisorption. The orbital energies of the deeper-lying NBOs of the phosphonyl group (HOMO-2 and HOMO-3) are computed to be 6.36 and 6.72 eV, respectively. Using the average for ε_H in the linear relationship obtained in Fig. 5 then gives ΔE_{ads} = -43.4 kcal/mol for adsorption on $Al_{32}O_{48}$. This compares reasonably well with the calculated value [4] of -39.2 kcal/mol.

5. Conclusions

Density functional theory has been applied to a study of the adsorption of a series of phosphonyl compounds on γ-Al_2O_3. The results are as follows.

(1) All the reagents studied adsorb *via* an Al–O=P dative bond at a coordinatively-unsaturated Al(T_d) site. Other possible modes of adsorption are energetically less favorable.
(2) The adsorption energy (ΔE_{ads}) shows a linear dependence on the difference between the one-electron orbital energies of the molecular HOMO (ε_H) and the Al(T_d) surface state (ε_S). Trends in ΔE_{ads} for different reagents on a given cluster, and for the same molecule on different clusters, can be understood quantitatively in terms of variations in ε_H and ε_S.
(3) Cluster models can be constructed which give ε_S in good agreement with two-dimensionally-periodic slab (2-DPS) predictions based on fundamentally-different models for the γ-Al_2O_3 bulk lattice. For test molecules such as H_2O and CO, properly-constructed clusters then give ΔE_{ads} results in good agreement with those from the corresponding 2-DPS calculations. Cluster models can thus be a viable alternative to 2-DPS calculations in the treatment of adsorption on a complex ionic oxide such as γ-Al_2O_3.
(4) The results may be extensible to other, non-phosphonyl species. For adsorption of CO *via* an Al–C=O bond, ΔE_{ads} values obtained from 2-DPS calculations agree well with cluster-model predictions based on a linear extrapolation of the phosphonyl results. Thus ΔE_{ads} for phosphonyls, and perhaps

for other species that adsorb by a similar dative-bond formation, can be estimated quantitatively using the easily-computed ε_H of the free molecule.

Acknowledgements

References

[1] M.B. Mitchell, V.N. Sheinker, E.A. Mintz, J. Phys. Chem. B 101 (1997) 11192.
[2] A.E.T. Kuiper, J.J.G.M. van Bokhoven, J. Medema, J. Catal. 43 (1976) 154.
[3] V.M. Bermudez, J. Phys. Chem. C 111 (2007) 3719.
[4] V.M. Bermudez, J. Phys. Chem. C, in preparation.
[5] A. Michalkova, M. Ilchenko, L. Gorb, J. Leszczynski, J. Phys. Chem. B 108 (2004) 5294.
[6] A. Michalkova, Y. Paukku, D. Majumdar, J. Leszczynksi, Chem. Phys. Lett. 438 (2007) 72.
[7] G. Klopman, J. Am. Chem. Soc. 90 (1968) 223.
[8] K. Fukui, Angew. Chem. Int. Ed. 21 (1982) 801.
[9] R. Hoffmann, Solids and Surfaces: A Chemist's View of Bonding in Extended Structures, VCH, Weinhiem, 1988.
[10] Gaussian 03, Revision D.02, M.J. Frisch, G.W. Trucks, H.B. Schlegel, G.E. Scuseria, M.A. Robb, J.R. Cheeseman, J.A. Montgomery, Jr., T. Vreven, K.N. Kudin, J.C. Burant, J.M. Millam, S.S. Iyengar, J. Tomasi, V. Barone, B. Mennucci, M. Cossi, G. Scalmani, N. Rega, G.A. Petersson, H. Nakatsuji, M. Hada, M. Ehara, K. Toyota, R. Fukuda, J. Hasegawa, M. Ishida, T. Nakajima, Y. Honda, O. Kitao, H. Nakai, M. Klene, X. Li, J.E. Knox, H.P. Hratchian, J.B. Cross, V. Bakken, C. Adamo, J. Jaramillo, R. Gomperts, R.E. Stratmann, O. Yazyev, A. J. Austin, R. Cammi, C. Pomelli, J.W. Ochterski, P.Y. Ayala, K. Morokuma, G.A. Voth, P. Salvador, J.J. Dannenberg, V.G. Zakrzewski, S. Dapprich, A.D. Daniels, M.C. Strain, O. Farkas, D.K. Malick, A.D. Rabuck, K. Raghavachari, J.B. 33 Foresman, J.V. Ortiz, Q. Cui, A.G. Baboul, S. Clifford, J. Cioslowski, B.B. Stefanov, G. Liu, A. Liashenko, P. Piskorz, I. Komaromi, R. L. Martin, D.J. Fox, T. Keith, M.A. Al-Laham, C.Y. Peng, A. Nanayakkara, M. Challacombe, P.M.W. Gill, B. Johnson, W. Chen, M.W. Wong, C. Gonzalez, and J.A. Pople, Gaussian Inc., Wallingford CT, 2004.
[11] G. te Velde, F.M. Bickelhaupt, E.J. Baerends, C. Fonseca Guerra, S.J.A. van Gisbergen, J.G. Snijders, T. Ziegler, J. Comput. Chem. 22 (2001) 931.
[12] W.A. Shapley, D.P. Chong, Int. J. Quantum Chem. 81 (2001) 34.
[13] H.B. Schlegel, J.J.W. McDouall, in: C. Ögretir, I.G. Csizmadia (Eds.), Computational Advances in Organic Chemistry: Molecular Structure and Reactivity, Kluwer, Dordrecht, 1991, p. 167.
[14] K.K. Irikura, R.D. Johnson III, R.N. Kacker, J. Phys. Chem. A 109 (2005) 8430.
[15] V.R. Saunders, R. Dovesi, C. Roetti, R. Orlando, C.M. Zicovich-Wilson, N.M. Harrison, K. Doll, B. Civalleri, I. Bush, Ph. D'Arco, M. Llunell, Crystal 2003 User's Manual, University of Torino, Torino, 2003. The manual and basis sets may be found at http://www.crystal.unito.it/.
[16] C. Pisani, R. Dovesi, C. Roetti, Hartree–Fock Ab Initio Treatment of Crystalline Systems, Springer, Berlin, 1988.
[17] J. Muscat, A. Wander, N.M. Harrison, Chem. Phys. Lett. 342 (2001) 397.
[18] H.P. Pinto, R.M. Nieminen, S.D. Elliott, Phys. Rev. B 70 (2004) 125402.
[19] C. Wolverton, K.C. Hass, Phys. Rev. B 63 (2000) 024102.
[20] G. Gutiérrez, A. Taga, B. Johansson, Phys. Rev. B 65 (2001) 012101.
[21] X. Krokidis, P. Raybaud, A.-E. Gobichon, B. Rebours, P. Euzen, H. Toulhoat, J. Phys. Chem. B 105 (2001) 5121.
[22] M. Digne, P. Sautet, P. Raybaud, P. Euzen, H. Toulhoat, J. Catal. 226 (2004) 54.
[23] M. Digne, P. Sautet, P. Raybaud, P. Euzen, H. Toulhoat, J. Catal. 211 (2002) 1.
[24] S.-H. Cai, S.N. Rashkeev, S.T. Pantelides, K. Sohlberg, Phys. Rev. B 67 (2003) 224104.
[25] G. Paglia, A.L. Rohl, C.E. Buckley, J.D. Gale, Phys. Rev. B 71 (2005) 224115.
[26] G. Paglia, E.S. Božin, S.J.L. Billinge, Chem. Mater. 18 (2006) 3242.
[27] E. Menéndez-Proupin, G. Gutiérrez, Phys. Rev. B 72 (2005) 035116.
[28] M. Sun, A.E. Nelson, J. Adjaye, J. Phys. Chem. B 110 (2006) 2310.
[29] A. Dyan, C. Azevedo, P. Cenedese, P. Dubot, Appl. Surf. Sci. 254 (2008) 3819.
[30] M. Digne, P. Raybaud, P. Sautet, B. Rebours, H. Toulhoat, J. Phys. Chem. B 110 (2006) 20719.
[31] G. Paglia, C.E. Buckley, A.L. Rohl, J. Phys. Chem. B 110 (2006) 20721.
[32] A.E. Nelson, M. Sun, J. Adjaye, J. Phys. Chem. B 110 (2006) 20724.
[33] S. Kim, D.C. Sorescu, O. Byl, J.T. Yates Jr., J. Phys. Chem. B 110 (2006) 4742.
[34] H. Knözinger, P. Ratnasamy, Catal. Rev. – Sci. Eng. 17 (1978) 31.
[35] M. Casarin, C. Maccato, A. Vittadini, Inorg. Chem. 39 (2000) 5232.
[36] Y.S. Li, M.M. Chen, J.R. Durig, J. Mol. Struct. 14 (1972) 261.
[37] L.M. Engelhardt, C.L. Raston, C.R. Whitaker, A.H. White, Austral. J. Chem. 39 (1986) 2151.

[38] R.D. Suenram, F.J. Lovas, D.F. Plusquellic, A. Lesarri, Y. Kawashima, O.J. Jensen, A.C. Samuels, J. Mol. Spectrosc. 211 (2002) 110.
[39] A.R.H. Walker, R.D. Suenram, A. Samuels, J. Jensen, M.W. Ellzy, J.M. Lochner, D. Zeroka, J. Mol. Spectrosc. 207 (2001) 77.
[40] A. Kaczmarek, L. Gorb, A.J. Sadlej, J. Leszczynski, J. Struct. Chem. 15 (2004) 517.
[41] V.M. Mamaev, E.V. Zernova, A.V. Prisyazhnyuk, E.M. Myshakin, D.V. Berdyshev, Dokl. Akad. Nauk. 349 (1996) 64. English transl.: Dokl. Phys. Chem. 349 (1996) 153.
[42] O.G. Strukov, S.V. Utkina, V.A. Petrunin, Z.V. Vlasova, I.V. Zavalishina, V.N. Fadeev, A.D. Kuntsevich, G.I. Drozd, Dokl. Akad. Nauk. 380 (2001) 784. English transl.: Dokl. Phys. Chem. 380 (2001) 247.
[43] S.M. Kanan, C.P. Tripp, Langmuir 17 (2001) 2213.
[44] L. Bertilsson, I. Engquist, B. Liedberg, J. Phys. Chem. B 101 (1997) 6021.
[45] F. Choplin, G. Kaufmann, Spectrochim. Acta 26A (1970) 2113.
[46] S. Chattopadhyay, G.L. Findley, S.P. McGlynn, J. Electron Spectrosc. Relat. Phenom. 24 (1981) 27.
[47] K.A. Ostoja Starzewski, H. tom Dieck, Inorg. Chem. 18 (1979) 3307.
[48] V. Dose, Surf. Sci. Rep. 5 (1985) 337.
[49] H. Kuhlenbeck, Appl. Phys. A 59 (1994) 469.
[50] R.M. Jaeger, H. Kuhlenbeck, H.-J. Freund, M. Wuttig, W. Hoffmann, R. Franchy, H. Ibach, Surf. Sci. 259 (1991) 235.
[51] I. Costina, R. Franchy, Appl. Phys. Lett. 78 (2001) 4139.
[52] R.H. French, J. Am. Ceram. Soc. 73 (1990) 477.
[53] C. Freysoldt, P. Rinke, M. Scheffler, Phys. Rev. Lett. 99 (2007) 086101.
[54] I.N. Yakovkin, P.A. Dowben, Surf. Rev. Lett. 14 (2007) 481.
[55] A. Jimenéz-Gonzaléz, D. Schmeisser, Surf. Sci. 250 (1991) 59.
[56] J.F. Janak, Phys. Rev. B 18 (1978) 7165.
[57] J. Robertson, B. Falabretti, J. Appl. Phys. 100 (2006) 014111.
[58] H. Iwasaki, K. Sudoh, Jpn. J. Appl. Phys. 41 (2002) 7496.
[59] K.H. Hansen, T. Worren, E. Lægsgaard, F. Besenbacher, I. Stensgaard, Surf. Sci. 475 (2001) 96.
[60] Y. Gu, T. Kar, S. Scheiner, J. Am. Chem. Soc. 121 (1999) 9411.
[61] P. Hobza, Z. Havlas, Chem. Rev. 100 (2000) 4253.
[62] M. Swart, P.Th. van Duijnen, J.G. Snijders, J. Comput. Chem. 22 (2001) 79.
[63] V.M. Bermudez, J. Phys. Chem. C 111 (2007) 9314.
[64] H.P. Pinto, S.D. Elliott, Mater. Res. Soc. Symp. Proc. 786 (2003) E5.21.
[65] A. Damin, R. Dovesi, A. Zecchina, P. Ugliengo, Surf. Sci. 479 (2001) 255.